

## Deformation Behavior and Microstructure Evolution of an Aircraft Al–Cu–Mg–Mn Alloy at the Elevated Temperature

Yujin. Huang, Zhiguo. Chen\*, Shicheng. Li, Wenling. Yang

School of Materials Science and Engineering, Central South University, Changsha, Hunan, Lushan South Road, 410083,  
The People's Republic of China

**Abstract:** The deformation behavior and microstructure evolution in a hot compressed 2E12 alloy has been investigated by constructing power dissipation map in which work efficiency can be related with microstructural evolution. The flow curves usually exhibited a peak followed by flow softening (deformation temperature within the range of  $250^{\circ}\text{C} \leq T \leq 450^{\circ}\text{C}$ ), which is caused by dynamic recovery. At  $500^{\circ}\text{C}$ , the flow curves showed the phenomenon of partial dynamic recrystallization. The processing maps revealed that two domains where dynamic recovery occurs comparatively: (1)  $325\text{-}400^{\circ}\text{C}$  and  $0.01\text{-}0.03\text{ s}^{-1}$ , (2)  $350\text{-}450^{\circ}\text{C}$  and  $1.78\text{-}10\text{ s}^{-1}$ ; and partial dynamic recrystallization occurs at  $500^{\circ}\text{C}$  and  $0.01\text{-}0.1\text{ s}^{-1}$ . Fine recrystallized grains were observed at  $500^{\circ}\text{C}$  for strain rate below  $0.1\text{ s}^{-1}$ , but only in local areas, near second phase particles, or at the as-received triple junctions. Finally, the processing route was recommended to obtain unrecrystallized and recrystallized microstructural versions of 2E12 alloy.

**Keywords:** Al alloy; deformation; microstructure

### 1. Introduction

2E12 alloy is independently developed as a relatively new aluminum alloy. It is prospected to be used in aerospace applications because of its high strength, high damage tolerance. However, today's aircraft and aerospace industry is requesting that longer lasting lives with lower maintenance costs programs running on existing aircraft versions which require new material solutions<sup>[1]</sup>. Thus, the correct identification of the 'processing window' (i.e. the combination of the temperature and strain-rate conditions that guarantee defect-free components) strongly affect their mechanical properties.

Dynamic Materials Model (DMM)<sup>[2-5]</sup> is available for analyzing the strain, strain rate, and temperature dependence of the flow stress. The model, when combined with proper processing--microstructure relationships and with failure criteria for the material, can help in defining and optimizing processing conditions to produce defect-free parts with controlled microstructures, and mechanical properties. The model considers the work piece to be a dissipater of power and the power might be instantaneously dissipated into two complementary parts—G content and J co-content<sup>[6]</sup>:

$$P = \bar{\sigma} \cdot \dot{\bar{\epsilon}} = G + J = \int_0^{\dot{\bar{\epsilon}}} \bar{\sigma} d\dot{\bar{\epsilon}} + \int_0^{\bar{\sigma}} \dot{\bar{\epsilon}} d\bar{\sigma} \quad (1)$$

where G represents the power dissipated by plastic work, most of which is converted into heat; the remaining small part is stored as lattice defects. The dissipator power co-content J is related to dynamic metallurgical processes, such as dynamic recovery, dynamic recrystallization, wedge cracking, etc.<sup>[7-12]</sup>. The power partitioning between G and J is controlled by the constitutive flow behavior of the material and is decided by the strain rate sensitivity (m) of flow stress, since

$$\frac{dJ}{dG} = \frac{\dot{\bar{\epsilon}} d\bar{\sigma}}{\bar{\sigma} d\dot{\bar{\epsilon}}} = \frac{d(\ln \bar{\sigma})}{d(\ln \dot{\bar{\epsilon}})} \approx \frac{\Delta \log \bar{\sigma}}{\Delta \log \dot{\bar{\epsilon}}} = m \quad (2)$$

\* Corresponding author, E-mail: hngary@163.com

For the workpiece acts as a linear dissipater ( $m=1$ ), in which maximum possible dissipation through  $J$  can occur ( $J_{\max} = \overline{\sigma\dot{\varepsilon}}/2$ ), leads to the definition of a dimensionless parameter, efficiency of power dissipation [13]:

$$\eta = \frac{J}{J_{\max}} = \frac{2m}{m+1} \quad (3)$$

This parameter and its variation with temperature and strain rate form the basis for the processing map. The efficiency represents the relative rate of internal entropy production during hot deformation and characterizes the dissipative microstructure at different temperature and strain rate conditions. The various domains in the maps may be correlated with specific microstructure processes. The aim of the present investigation is to study the deformation processing of 2E12 alloy with a view to establishing an interrelation between the process parameters (temperature and strain rate) and the microstructure. In this study, the interrelation between processing parameters and microstructure has been established; the proper processing parameters-controlled mechanical properties relationships could be expected on the base.

## 2. Experimental procedure

The alloy used in this investigation has been semi-continuously cast and homogenized at 490°C for 24 h. The chemical primary composition (in wt. %) is Al-4.45Cu-1.50Mg-0.54Mn. Cylindrical specimens of 10-mm diameter and 15-mm height were machined from the homogenized ingot for compression. Concentric grooves of about 0.2-mm depth were engraved on both end faces to facilitate the retention of the lubricant. Graphite lubricant mixed with machine oil was used to minimize the friction.

Hot compression tests were conducted in the temperature range of 250-500°C at 50°C intervals and constant true strain rate ranging from 0.01 to 10 s<sup>-1</sup> at intervals of an order of magnitude. All samples were heated up to test temperature at the speed of 120 °C /min and hold for 5 min to prevent a volumetric change due to thermal expansion before compression. The flow stress data obtained at different temperatures, strain rates and strains have been corrected for the influence of adiabatic temperature rise were corrected by assuming a linear relation of log $\sigma$  and 1/T over intervals of 50 °C. All specimens were deformed to true strain of  $\varepsilon = 0.51$  and water quenched from the test temperature. The compression direction was parallel with axis of the specimens. The deformed specimens were sectioned parallel to the compression axis and the microstructure observation was conducted by using Electron Backscattered Diffraction (EBSD).

## 3. Results and Discussion

### 3.1 True stress-true strain

Typical stress-strain curves recorded at strain rate of 0.01 s<sup>-1</sup> and 10 s<sup>-1</sup> at different temperatures for 2E12 alloy were showed in Fig. 1 (a) and (b), respectively. Flow stress decreases as the temperature rises and strain rate drops. At strain rates lower than 10 s<sup>-1</sup>, most of flow curves showed the steady state flow, possibly, due to the high stacking fault energy of Al and its alloys. The flow curves exhibit nearly steady state behavior and the critical strain to the steady state increases with strain rate increase and temperature decrease. Under the condition of strain rate of 10 s<sup>-1</sup> and 450°C ≤ T ≤ 500°C, the flow stress curves exhibit a remarkable peak stress which may caused by dynamic recrystallization or flow instability [14]. It is impossible to identify the mechanisms of hot working directly from the shape of the true stress-true strain curves alone since the flow curves may be the result of the interaction of several mechanisms such as dynamic recovery, dynamic recrystallization, internal fracture (void formation or wedge cracking), dissolution or growth of

particles or phases under dynamic conditions, dynamic spheroidization of acicular structures, and deformation-induced phase transformation or precipitation under dynamic conditions<sup>[5]</sup>.

The microstructure could be evolved into various ways depending on the deformation conditions. So the precise hot deformation mechanism of 2E12 alloy will be identified by processing maps combined with microstructural observations.

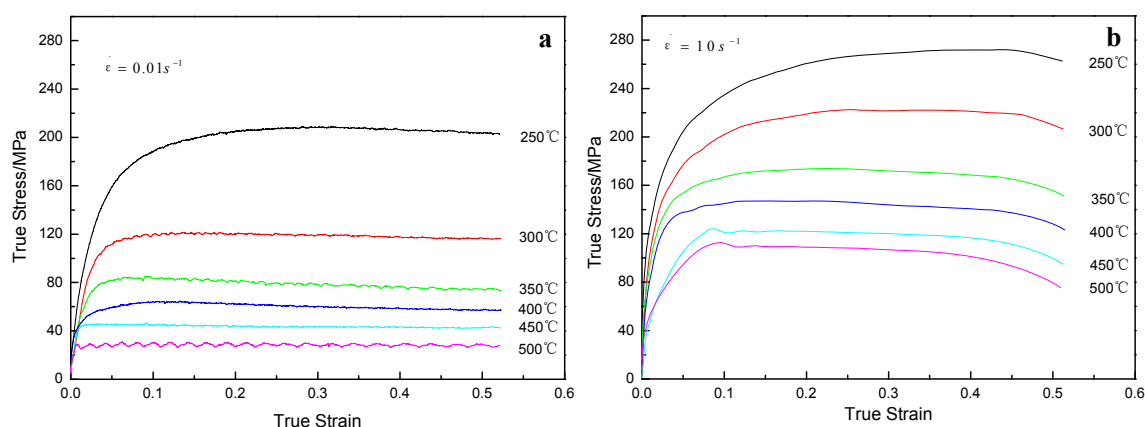


Fig.1. Typical flow curves obtained from compression test on 2E12 alloy at (a)  $0.01\text{s}^{-1}$  and (b)  $10\text{s}^{-1}$  for different temperatures

### 3.2 Processing maps

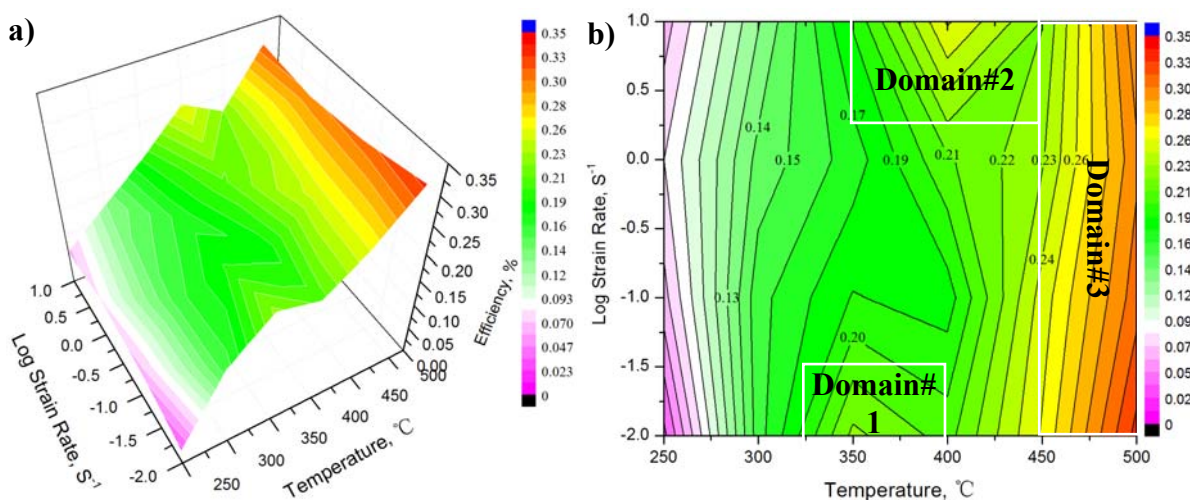


Fig.2. (a) Three-dimensional plot showing the variation of efficiency of dissipation with temperature and strain rate for 2E12 alloy at a strain of 0.3, (b) Contour map with iso-efficiency contours of the efficiency of power dissipation for 2E12 alloy corresponding to the 3-D map.

The flow stress is corrected for the adiabatic temperature rise and this correction was found to be significant at lower temperatures and higher strain rates. For example, the temperature increment reaches to the maximum  $45\text{ }^{\circ}\text{C}$  when the alloy was deformed at  $250^{\circ}\text{C}$  and  $10\text{ s}^{-1}$ .

Power dissipation maps were constructed using the data described above and the principles of the DMM<sup>[6]</sup>. This model is a continuum one and follows a systems approach. The efficiency of power dissipation representing microstructural changes  $[\eta=2m/(m+1)]$  is then calculated from a set of  $m$  values as a function of strain rate and temperature and plotted as a three-dimensional (3-D) map. The power dissipation map at a strain of 0.3 is shown in Fig.2 (a) in 3-D and in Fig.2 (b) as a contour map filled with colors. A strain of 0.3 is selected, since this value is large enough to effect homogeneous deformation and small enough to minimize the influence of barreling.

The maps for 2E12 alloy exhibited three domains with higher value of power dissipation: Domain #1 occurs in the temperature range of 325-400°C and strain rate range of 0.01-0.03 s<sup>-1</sup>, with a peak efficiency of about 22% at about 350 °C and 0.01s<sup>-1</sup>. Domain #2 occurs in the temperature range of 350-450 °C and strain rate range of 1.78-10s<sup>-1</sup>, with a peak efficiency of about 25% at 400 °C and 10s<sup>-1</sup>. Domain #3 occurs in the temperature range of 450-500 °C and strain rate range of 0.01-10s<sup>-1</sup>, with a peak efficiency of about 33% at 500 °C and 0.01s<sup>-1</sup>.

The power dissipation maps are continuum maps; however, the domains can be interpreted in terms of specific atomistic processes. This can be done with the help of Raj maps [15]. In hot deformation, there are "safe" and "unsafe" mechanisms that occur at different strain rate and temperature combinations. The safe mechanisms are dynamic recovery (lower temperature and strain rates) and dynamic recrystallization (higher temperature and intermediate strain rates). Microstructural damage due to wedge cracking will occur at intermediate strain rates; void formation at hard particles is dominant at high strain rates and low temperatures. The damage processes are very efficient in dissipating power through the generation of new surfaces, while the "safe" processes are less efficient, since power dissipation occurs by annihilation of dislocations or their groups. Out of the two safe processes, dynamic recrystallization has a higher efficiency than dynamic recovery.

### 3.3 Microstructural Evolution

The initial microstructure of the as-received material showed equi-axed grains with large particles at the grain boundaries. The grain interiors with a low dislocation density were observed to be filled with various kinds of particles. The average grain diameter is about 20µm.

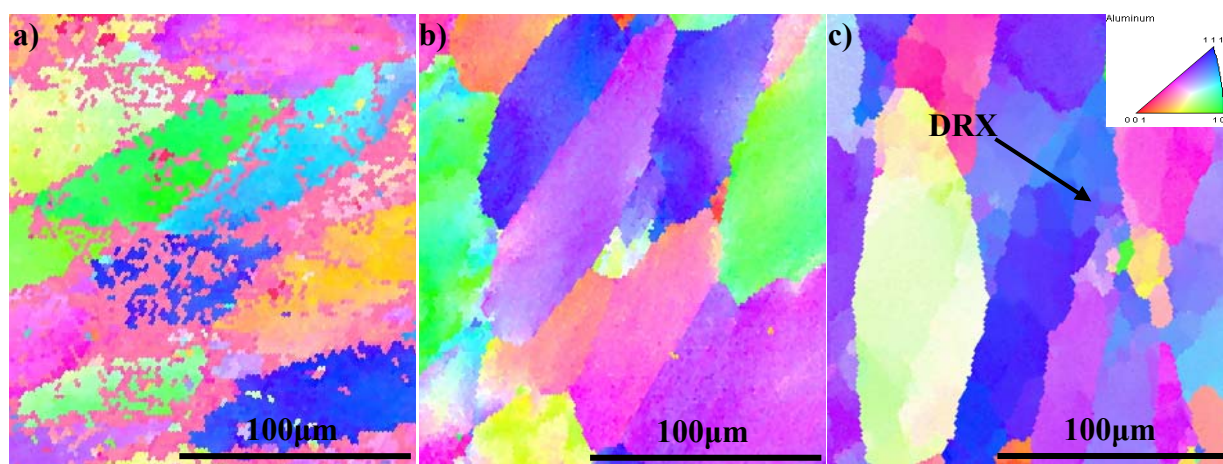


Fig.3. EBSD map of 2E12 alloy hot deformed at different condition: (a) 350°C and 0.01s<sup>-1</sup>; (b) 450°C and 10s<sup>-1</sup>; (c) 500 °C and 0.1s<sup>-1</sup>.

On the basis of the above interpretation, the domains observed in the power dissipation maps of 2E12 alloy represent the process of dynamic recrystallization and has a maximum efficiency of 22 to 33 pct. This interpretation is further confirmed by the micro-structural observations.

After deformation at 350°C and 10<sup>-2</sup> s<sup>-1</sup>; or 450°C and 10s<sup>-1</sup>, the microstructures were similar in spite of the large differences in flow stress level and in stress-strain behavior. Compared with the as-annealed microstructures, the microstructure consists of pancake-shaped grains. With strain rate rising to 10s<sup>-1</sup>, the grains were more elongated. There is no evidence of recrystallization at this stage (Fig.3 (a) and (b)).

Compression at 500°C resulted in a gradual change in microstructure, which exhibits very fine equiaxed grains, were seen in local regions indicating that either static or dynamic recrystallization had occurred, presumably because of the locally higher strain and strain rate at the triple junctions or in the vicinity of the particles (Fig. 3(c)). The flow curve corresponding to this region exhibits flow stress softening with remarkable periodic peak, and the efficiency of power dissipation in this domain reaches above 30%.

With strain rate rising above  $1\text{ s}^{-1}$ , the heat generated during deformation cannot dissipate rapidly and temperature rise is inevitable [16]. After being compressed at  $500^\circ\text{C}$  and  $1\text{ s}^{-1}$ , because of deformation heating, resulted in final test temperatures above the solidus temperature ( $502^\circ\text{C}$ ), the microstructure of the specimen revealed the partial redissolution of large particles, which was also observed by Chrspentier [17], and the presence of intercrystalline cracks, which was also found in pure aluminum by Prasad [18] for  $500^\circ\text{C}$ . It is possible that these cracks initiated at grain boundary triple junctions where the partial redissolution of partials happened consequent to grain boundary sliding.

#### 4. Conclusions

1. The processing maps revealed that two domains where dynamic recovery occurs comparatively: (1)  $325\text{-}400^\circ\text{C}$  and  $0.01\text{-}0.03\text{ s}^{-1}$ , (2)  $350\text{-}450^\circ\text{C}$  and  $1.78\text{-}10\text{ s}^{-1}$ ; and partial dynamic recrystallization occurs at  $500^\circ\text{C}$  and  $0.01\text{-}0.1\text{ s}^{-1}$ .

2. There was evidence of redissolution of the particles and intercrystalline cracks at  $500^\circ\text{C}$  and  $1\text{-}10\text{ s}^{-1}$ . Fine recrystallized grains were observed at  $500^\circ\text{C}$  for strain rate below  $0.1\text{ s}^{-1}$ , but only in local areas, near second phase particles, or at the as-received triple junctions.

3. It was also found that there would be a wide region where recovery process dominates during deformation in the present alloy for an industrially applicable processing because the efficiency level was quite uniform in the temperature range of  $300^\circ\text{C}$  -  $450^\circ\text{C}$  and the examined strain rate range.

#### Acknowledgements

This work was financially supported by the National Natural Science Foundation of China (Grant No.50871123) and National Program on Key Basic Research Project (Grant No. 2005CB623705).

#### References

- [1] A. Heinz, A. Haszler, C. Keidel, et al: Mater. Sci. Eng. A280(2000)102–107.
- [2] K.P. Rao, Y.V.R.K. Prasad: Journal of Materials Processing Technology 201 (2008)359-363.
- [3] S. Spigarelli: Mater. Sci. and Eng. A327 (2002)144-154.
- [4] Meng Gang, Li Bolong, Li Hongmei, et al: Mater. Sci. Eng. A516(2009)131-137.
- [5] Y. V. R. K. Prasad, H.L. Giegel, S.M. Dorraivelu, et al: Metal. Trans. A, 15A(1984)1883-1892.
- [6] Y.V.R.K. Prasad, K.P. Rao: Mater. Sci. and Eng. A391(2005)141-150.
- [7] Y.V.R.K. Prasad: Mater. Sci. Eng. A487(2008)316-327.
- [8] O. Sivakesavam, Y.V.R.K. Prasad: Mater. Sci. Eng. A362 (2003)118-124.
- [9] Y.V.R.K. Prasad, S. Sasidhara: Intermetallics 8(2000)987-995.
- [10] C.Y.Wang, K.Wu: Mater. Sci. Eng. A477(2008)179-184.
- [11] Y.V.R.K. Prasad: Mater. Sci. Eng. A311(2001)42-53.
- [12] Y.V.R.K. Prasad, T. Seshachayulu: Inter. Mater. Rev. 44(1998)243-258.
- [13] S. V. S. Narayana Murty, B. Nageswara Rao, et al: Inter. Mater. Rev. 45(2000) 15-26.
- [14] S.V.S. Narayana Murty: Materials Processing Technology 104(2000)103-109.
- [15] R. Raj: Metall. Trans. A, 12A(1981)1089-97.
- [16] A. Laasraoui and J.J. Jonas: Metall Trans. 22A(1991)1545-1558.
- [17] P.L. Chrspentier, B.C. Stone, S.C. Ernst, et al: Metall Trans. 17A(1986)2227-2237.
- [18] N. Ravichandran and Y.V.R.K. Prasad: Metall Trans. 22A(1991)2339-2348.